Sustainable Energy & Fuels

ROYAL SOCIETY OF CHEMISTRY

PAPER

View Article Online
View Journal | View Issue

Cite this: *Sustainable Energy Fuels*, 2024, **8**, 1679

Cobalt-based metal–organic framework for desulfurization of thiophene as a model fuel†

M. Christina Nilavu, T. Leelasree, Himanshu Aggarwal* and N. Rajesh *

Persistent economic growth results in rising energy use, which in turn creates new environmental burdens and health risks for people due to the release of toxic gases from the combustion of fuel with sulfur-containing compounds. A cobalt-based MOF (BITSH-1) was investigated for the adsorptive desulfurization of thiophene in iso-octane as a model fuel. BITSH-1 showed a very high thiophene adsorption capacity of 95.38 mg g^{-1}. Interestingly, BITSH-1 with a high surface area of 349.07 m^2 g^{-1} achieves high adsorption efficiency at room temperature with substantially less time consumption without fuel oxidation or additional functionalization of the MOF, making it more feasible for an adsorptive desulfurization process. The recyclability of the MOF material showed good adsorption efficiency of thiophene for up to four cycles. The mechanistic features and possible interactions are discussed by modelling the thiophene molecule in the MOF with the help of SCXRD studies. Additionally, the mechanistic aspects of thiophene adsorption were corroborated using isotherms, kinetics, and thermodynamics, which ascertained that the reaction follows pseudo-order kinetics with spontaneity and feasibility. The overall process was found to be an exothermic reaction. Hence, the proposed adsorbent BITSH-1 could be a promising candidate for exclusive thiophenic separation from oil and could be promoted for the desulfurization of thiophenic model fuel.

Received 31st August 2023
Accepted 24th February 2024

DOI: 10.1039/d3se01140b

rsc.li/sustainable-energy

1. Introduction

Fossil fuels are crucial to the advancement of research, technology, and daily lives. Nearly half of the energy from fossil fuels is provided by petroleum in the form of liquid fuel. Aromatic sulfur compounds in the fuel tend to release toxic gases, such as SO_2 and SO_3, on account of combustion in vehicles, impacting the ecosystem through consequences such as acid rain. SO_2 emissions also induce respiratory ailments and early human mortality due to deteriorating air quality.[1] Apart from pollution and health effects, high levels of sulfur content reduce the efficiency of a vehicle engine.[2] According to BS(VI) emission regulations, the level of sulfur in fuel is expected to be below 10 mg L^{-1}.[1–3] The existence of sulfur in numerous forms with different properties, such as variance in size, reactivity, and polarity, makes desulfurizing fuel cumbersome. Due to their non-polar character and great stability, thiophene and its derivatives are more prevalent than aliphatic forms in petrol and are also harder to remove. Desulfurization of gasoline is an environmental challenge to be addressed on a large scale.

Extractive desulfurization, bio-desulfurization, oxidative desulfurization, and adsorptive desulfurization are common approaches to desulfurization. However, these procedures have certain lacunae, such as the identification and use of organic solvents in extractive desulfurization, the instability of microorganisms at higher temperatures, and selectivity, which acts as impediments beyond the laboratory scale. High temperatures and the requirement for oxidants in the process of oxidative desulfurization also limit its usefulness.[4] At the industrial level, the conventional method used is hydrodesulfurization, but requirements such as high temperature and pressure and an expensive setup restrict its application.[5,6] However, adsorptive desulfurization can be advantageous over above-mentioned methods in terms of recyclability of adsorbent, high selectivity towards the targeted compound, tailorable functional properties and cost-effectiveness. It offers an alternative route for desulfurization technology considering the likelihood of physical and chemical interactions between the adsorbent and targeted adsorbate, as well as the removal of sulfur at room temperature without the consumption of additional energy.[7] Proposed adsorbents for desulfurization include activated carbon, modified, functionalized and heteroatom-doped carbon, zeolites, graphitic materials, metal oxide composites and metal–organic frameworks (MOFs).[8,9]

Metal–organic frameworks (MOFs) are porous crystalline materials that combine organic and inorganic building blocks into a periodic networked structure. The porous nature and

Department of Chemistry, Birla Institute of Technology and Science-Pilani, Hyderabad Campus, Jawahar Nagar, Hyderabad 500078, India. E-mail: nrajesh@hyderabad.bits-pilani.ac.in; himanshu.aggarwal@hyderabad.bits-pilani.ac.in

† Electronic supplementary information (ESI) available. CCDC 2289319. For ESI and crystallographic data in CIF or other electronic format see DOI: https://doi.org/10.1039/d3se01140b

high specific area of MOFs make them suitable candidates for application in catalysis, sensing and separation technologies, and in gas adsorption studies.[10] The pore size in MOFs could be fine-tuned by functionalization of the organic linkers towards achieving the selective adsorption of guest molecules. Additionally, MOFs possess a regular network of metal and organic moieties, which creates a cage-like structure with a sizable pore volume, increasing the likelihood of physisorption and chemisorption. Thus, separation by an adsorptive method is in vogue for MOF materials compared to other adsorbents, such as activated carbon,[6,11] modified, functionalized or heteroatom-doped carbon,[12] zeolites,[13] graphitic materials,[14] and metal oxide composites.[12]

MOFs have been investigated for desulfurization processes because of their advantages in terms of porosity, stability, and optimum pore sizes. However, only a few MOF structures have been explored for adsorptive desulfurization, and most of these materials display limited capacity for adsorption. Previously reported Cu-based MOFs such as MOF-199 showed a capacity of 18 mg g^{-1} for thiophene and 1.85 mg g^{-1} for sulfur from dibenzothiophene (DBT). Fe- and Cr-based MOFs were reported to have adsorption capacities of 6.50 and 32 mg g^{-1} for the adsorptive desulfurization of DBT. Modification of MIL-101 Cr with phosphotungstic acid (PTA) was found to give a higher adsorptive capacity of 107 mg g^{-1}. CuCl modified MIL-101 Cr gave an adsorption capacity of 18.4 mg g^{-1}. HKUST-1 gave an adsorption capacity of 40.6 mg g^{-1} for 500 μL of benzothiophene (BT) of 1500 mg L^{-1} concentration.[13,15,16] In this study, we have explored a cobalt-based MOF (BITSH-1) for the adsorptive desulfurization of thiophene at room temperature without any modification or functionalization of the MOF. BITSH-1 was also explored for the adsorptive desulfurization of benzothiophene (BT) and dibenzothiophene (DBT) to check its selectivity with similar sulfur-based compounds present in the fuel.

2. Results and discussions

2.1. MOF synthesis and characterization

BITSH-1 was synthesized solvothermally using a mixed linker approach by reacting cobalt metal salt with biphenyl-4,4-dicarboxylic acid (BPDC) and 4,4′-bipyridine (BPY)[17] (as given in Fig. 1a). BITSH-1 crystallizes in the $P2_1/n$ space group with the asymmetric unit containing three cobalt (Co^{2+}) ions, three BPDC linkers, one BPY linker and a water molecule. The as-synthesized material showed good crystallinity and bulk phase purity (Fig. S2†). TGA analyses were performed to study the thermal stability of the MOF material. The MOF material was thermally stable up to 350 °C (as shown in Fig. S4a†). N_2 sorption isotherms of BITSH-1 were collected at 77 K. BITSH-1 displayed a microporous nature with a surface area of 349.07 m^2 g^1 and a pore diameter of 8 Å (Fig. S3b†). The high surface area along with the suitable pore size of BITSH-1 enabled us to explore this MOF for the adsorption of analytes with a desirable size up to 8 Å. Thiophene with a kinetic diameter of 4.5 Å (ref. 18) can be easily adsorbed onto BITSH-1 MOF pores. Thus, we proceeded further for the adsorptive desulfurization of

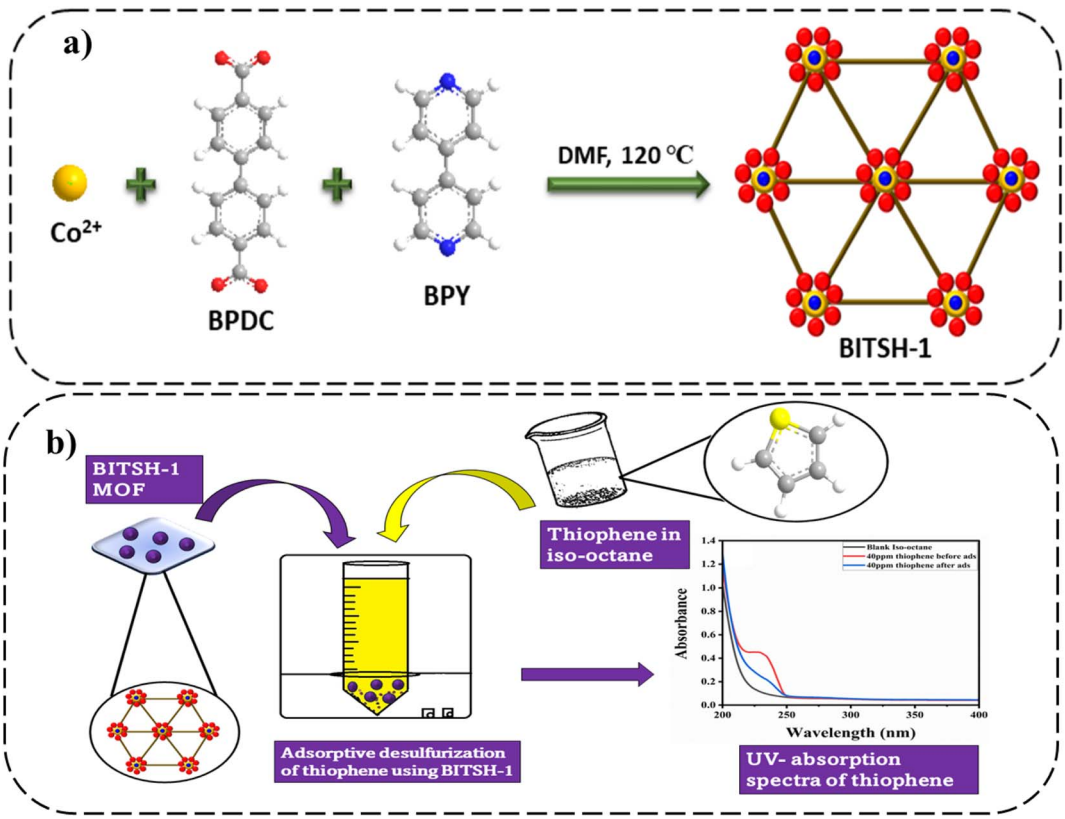

Fig. 1 (a) Synthesis scheme for BITSH-1. (b) Scheme for the adsorption and analysis of thiophene.

thiophene. The morphology and surface nature of BITSH-1 were studied using SEM. SEM images showed distinct crystals of BITSH-1 MOF with a crystallite size of 70 to 190 μmm in a block shape. Elemental mapping and EDX confirmed the presence of Co, C, N, and O elements and the absence of S element in BITSH-1. However, sulfur was found to be present in the sample after the adsorptive desulfurization experiment (Fig. S1a–l†).

2.2. Adsorptive studies of BITSH-1 for the desulfurization of thiophene

2.2.1. Adsorption procedure and thiophene analysis. The porous network of BITSH-1 with its high specific area was used for the adsorptive desulfurization of a model fuel (thiophene in iso-octane). The removal of thiophene was quantified using UV-Vis spectra, where thiophene showed a λ_{max} at 233 nm. The calibration plot for thiophene for different concentrations is given in Fig. 1a. To perform the adsorption experiment, 40 mg L^{-1} of thiophene in iso-octane with 20 mg of BITSH-1 MOF was kept in an incubator shaker for 3 h at 100 rpm (as shown in Fig. 1b). After the adsorption process, the residual concentration of thiophene in the solution was quantified using UV-Vis spectra, as shown in Fig. 2(a) and (b).

2.2.2. Adsorbent dosage studies. The effect of adsorbent dosage on adsorption efficiency was studied by varying the amount of BITSH-1 adsorbent from 5.0 mg to 40 mg for 50 mg L^{-1} thiophene in 10 mL of thiophene in iso-octane. The effect of the adsorbent was linearly plotted against the percentage adsorption efficiency, as shown in Fig. 3a. From the plot, it was observed that the percentage adsorption efficiency increased linearly with the rise in adsorbent dosage. This is attributed to the fact that an increase in the weight of the adsorbent would enhance active sites available for adsorbing thiophene molecules more efficiently. In addition, the probable interactions of the MOF material with thiophene in the system increase with an increase in the adsorbent dosage, enhancing the adsorption capability of the MOF.

2.2.3. Isotherm studies. The interaction and distributions of the thiophene molecules on BITSH-1 MOF can be characterized by classical isotherm models. The isotherm studies were performed with a 10 mL volume of 50–500 mg L^{-1} thiophene in iso-octane with 20 mg of adsorbent (BITSH-1 MOF) for 3 h in an orbital shaker at 100 rpm. The experimentally obtained isotherm results were fitted to different isotherm model equations.

The Langmuir isotherm model gives the maximum adsorption capacity of the adsorbent from the linearly fitted values of experimental data in the linear equation,[19]

$$\frac{C_e}{q_e} = \frac{1}{q_{max}} C_e + \frac{1}{K_L q_{max}} \quad (1)$$

where C_e and q_e are the initial and equilibrium concentrations of thiophene solution, and q_{max} is the maximum adsorption capacity of the adsorbent calculated from the slope ($1/q_{max}$) of the plot of C_e/q_e against q_e, as given in Fig. 4b. R_L is a dimensionless constant calculated as,[20]

$$R_L = \frac{1}{1 + C_0 K_L}, \quad (2)$$

where C_0 is the initial concentration of thiophene, and K_L is the Langmuir constant. An R_L value, or the separation factor, in the range $0 < R_L < 1$ specifies the favourability of the adsorption process, whereas $R_L = 0$ or $R_L > 1$ specifies the unfavorability and irreversibility of the adsorption system.[21] From the theoretical data of thiophene adsorption on BITSH-1, R_L was found to be 0.490, indicating that the adsorption is favourable. From the plot in Fig. 3b, the calculated maximum adsorption capacity was found to be 95.438 mg g^{-1} with an R^2 value of 0.966.

The Freundlich linear isotherm model can be given as,[22]

$$\log q_e = \log K_F + \frac{1}{n} \log C_e \quad (3)$$

$\log K_f$ is the intercept value obtained by plotting $\log C_e$ *vs.* $\log q_e$ (Fig. 3c). K_f is the Freundlich constant, and the $1/n$ value (the slope) depicts the intensity of adsorption or the heterogeneity of the surface of the adsorbent since the Freundlich isotherm corresponds to multilayered adsorption on heterogenous sites.

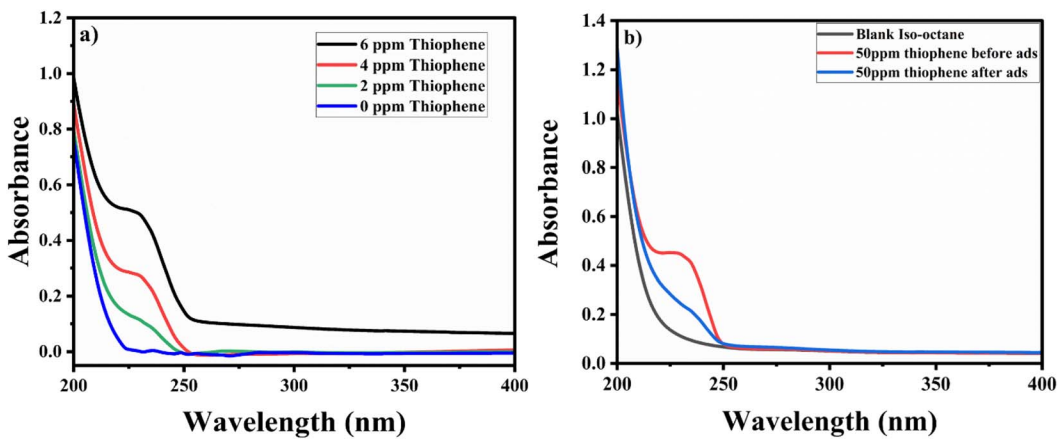

Fig. 2 (a) UV-Vis absorption spectra of different concentrations of thiophene with λ_{max} at 233 nm (0 to 6 mg L^{-1}). (b) UV-Vis absorption spectra of thiophene before and after adsorption.

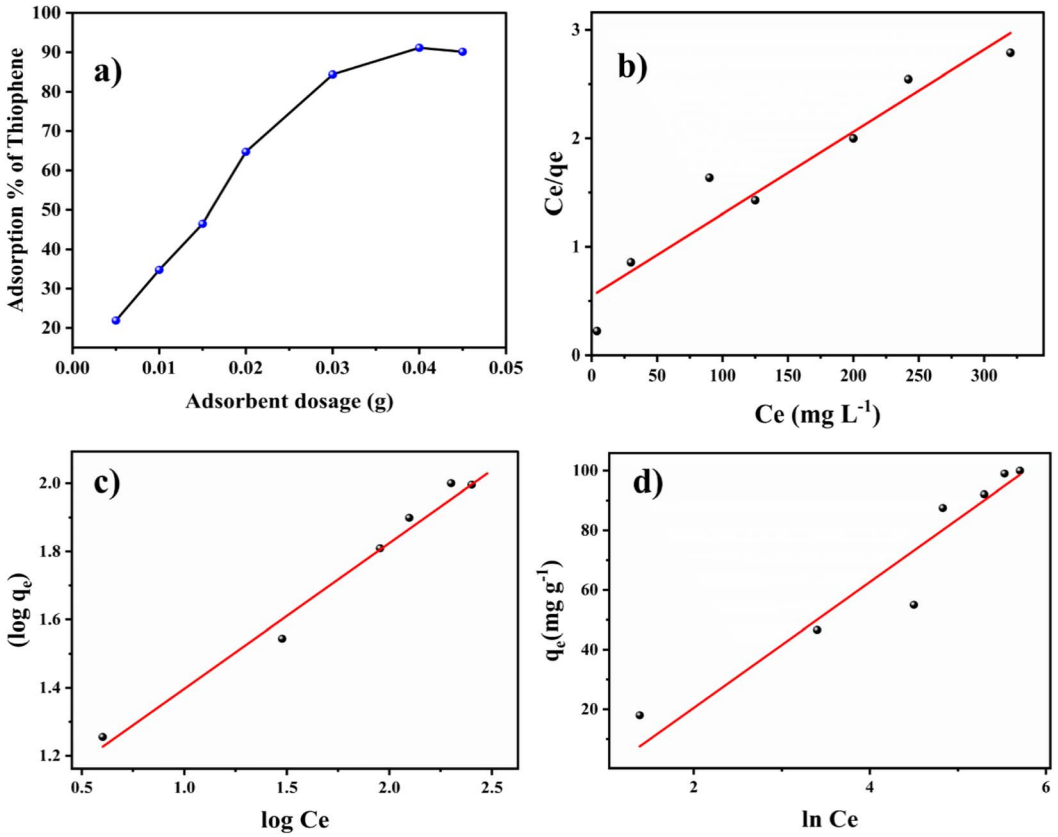

Fig. 3 (a) Adsorbent dosage effect of BITSH-1. (b) Langmuir isotherm model, (c) Freundlich isotherm model and (d) Temkin isotherm model.

A $1/n$ value < 1 specifies the favourability of linear adsorption, whereas $1/n > 1$ shows the unfavourability, and when $1/n = 1$, it corresponds to the irreversible nature of the process. For thiophene adsorption on BITSH-1, $1/n$ was found to be 0.427, confirming the favourability of the adsorption. The R^2 value for the Freundlich model was 0.954.

The linear Temkin isotherm equation is given as,[23]

$$q_e = \frac{RT}{b_{Te}} \ln K_T + \frac{RT}{b_{Te}} \ln C_e, \quad (4)$$

where R is the gas constant, K_T is the Temkin constant and b_{Te} is a constant parameter calculated by plotting $\ln C_e$ *vs.* q_e (Fig. 3d), which is related to the heat of adsorption in units of J mol^{-1}, and T is the temperature in Kelvin. The assumption of the Temkin isotherm specifies homogeneity in the distribution of binding energy over the adsorbent BITSH-1 throughout the process provided it also specifies that the heat of adsorption tends to reduce with an increase in the occupancy of the thiophene molecules on BITSH-1 MOF throughout the process.[24] The R^2 value for the Temkin model was 0.881.

The above mentioned theoretically obtained isotherm parameters from the experimental data are listed in Table S1.† Comparing the R^2 values of the three isotherm models, the Langmuir isotherm model shows the highest value of 0.966, confirming that the adsorption of thiophene on BITSH-1 follows and adheres to the Langmuir isotherm model pertaining to monolayer adsorption. As the BET isotherm data shows type 1 isotherm adsorption of thiophene on BITSH-1, it clearly follows monolayer adsorption since it is a microporous material where the pore size is not much larger than the size of the adsorbate molecule (thiophene) which has a size of 4.5 Å. Therefore, these narrow pores get completely filled, corresponding to the complete formation of a molecular monolayer during the adsorption process.

2.2.4. Kinetic studies for the adsorption of thiophene on BITSH-1. Kinetic studies were performed to further optimize and elucidate the mechanistic view of thiophene adsorption on BITSH-1. For the kinetic experiment, 50 mg L^{-1} of 10 mL of thiophene in iso-octane with 20 mg of adsorbent was kept for adsorption in an orbital shaker for 3 h, and the concentration of thiophene was checked for absorbance at equal time intervals. The adsorption efficiency of thiophene on BITSH-1 was plotted against the contact time (as given in Fig. 4d). It was observed that the percentage adsorption efficiency increased with an increase in the contact time of thiophene and BITSH-1, reaching an equilibrium of 90% after 3 h.

The experimental data was plotted as different kinetic models according to following equations. The pseudo-first-order and pseudo-second-order equations can be linearly expressed as,[25]

$$\log(q_e - q_t) = \log(q_e) - \frac{k_1}{2.303} t \quad (5)$$

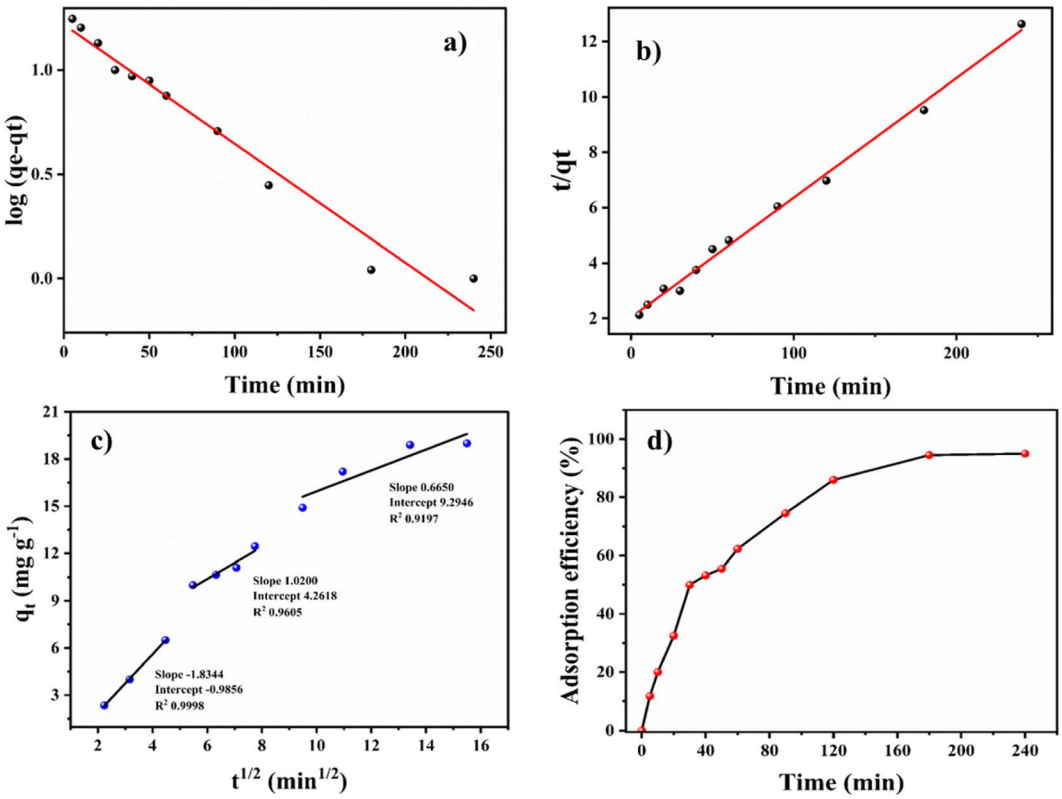

Fig. 4 (a) Pseudo-first-order kinetics, (b) pseudo-second-order kinetics, (c) Weber–Morris intra-particle diffusion model. (d) Effect of contact time of BITSH-1 adsorbent on adsorption efficiency.

$$\frac{t}{q_t} = \frac{1}{k_2 q_e^{\,2}} + \frac{t}{q_e} \tag{6}$$

The pseudo-first-order model (Fig. 4a) was plotted between time (min) and $\log(q_e - q_t)$, and the pseudo-second-order model (Fig. 4b) was plotted between time (min) and t/q_t. Here, q_e and q_t are the adsorption capacities at equilibrium and at a given time t, respectively. The R^2 values for the pseudo-first-order kinetics was 0.964 and for pseudo-second-order was 0.995. The q_e values obtained theoretically from the slope of the equations for first-order and second-order were 16.541 mg g^{-1} and 19.998 mg g^{-1}. The experimental q_e value was 20 mg g^{-1}. Therefore, the q_e value obtained from the second-order was found to be closer to the experimental q_e value, ascertaining that the adsorption of thiophene follows pseudo-second-order kinetic with a higher R^2 value as well. The theoretically obtained calculated data for kinetic parameters are listed in Table S2.†

An intra-particle diffusion plot for the adsorption process was drawn (given in Fig. 4c), between the square root of t and q_t. The intra-particle diffusion model showed three stages of linear plot for the adsorption. The first stage of the three involves the diffusion and transfer of mass from the boundary layer to the bulk phase. This is followed by the diffusion of thiophene through the boundary layer to the surface of the BITSH-1 MOF. Then, the third step is interaction with functional groups along with the π–π interaction between thiophene and BITSH-1.[26] The parameters of the Weber–Morris model were derived from the equation,

$$q_t = k_i t^{1/2} + C \tag{7}$$

2.2.5. Thermodynamic studies for the adsorption of thiophene on BITSH-1. Since adsorption is a temperature-dependent process, investigations into its thermodynamics provide a deeper understanding of the mechanistic approach. To determine the spontaneity and viability of such processes, thermodynamic considerations are necessary for adsorption experiments. A thermodynamic study was performed with 50 mg L^{-1} concentration of 10 mL of thiophene in iso-octane with an adsorbent weight of 20 mg for 3 h in an orbital shaker at different temperatures of 298, 308, 318 and 328 K. The thermodynamic parameters (listed in Table S4†), such as ΔG, ΔH, and ΔS, were calculated using the slope and intercept of the Van't Hoff plot (Fig. 6a) between $1/T$ and $\ln K_{eq}$, where the linear form of the equation is,

$$\Delta G^\circ = -RT \ln K_{eq} \tag{8}$$

$$\ln K_{eq} = -\frac{\Delta H^\circ}{R}\left(\frac{1}{T}\right) + \frac{\Delta S^\circ}{R} \tag{9}$$

The positive slope of the Van't Hoff plot specifies the exothermic nature of the reaction. The negative value of ΔS,

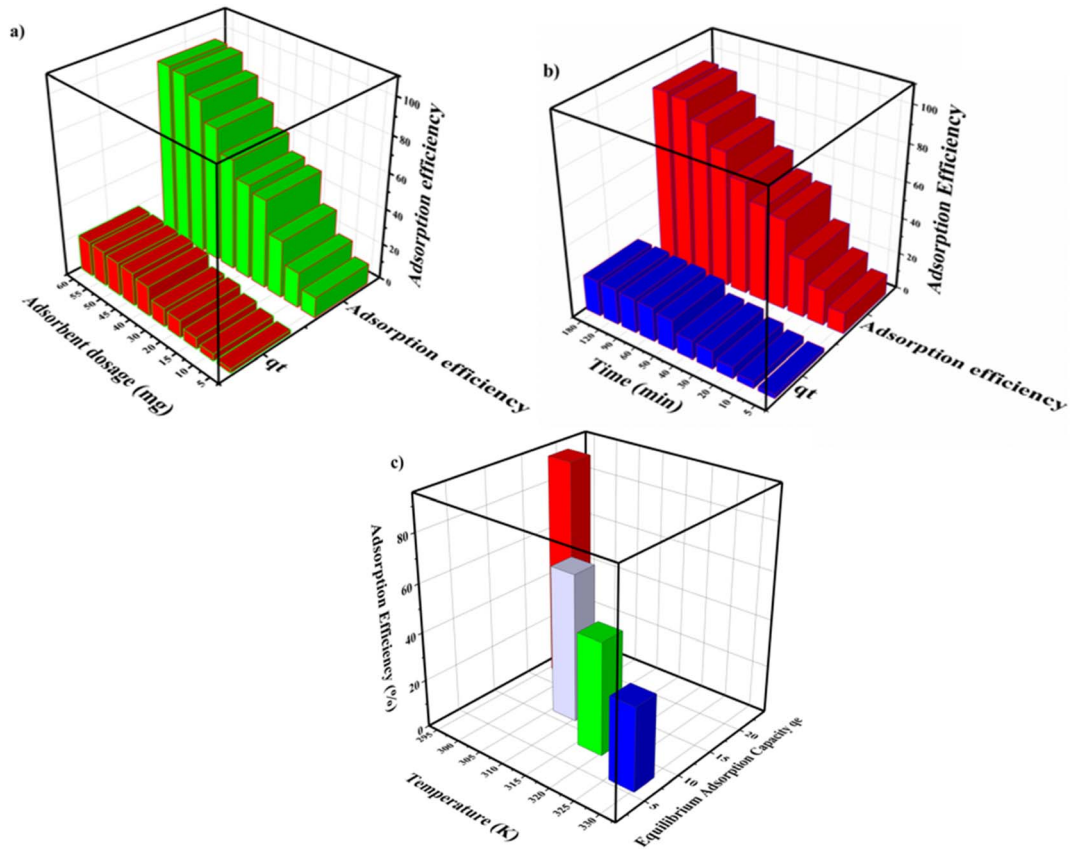

Fig. 5 3D plots of adsorption efficiency controlled by different parameters: (a) adsorbent dosage, (b) time and (c) temperature.

-0.276 kJ mol^{-1} indicates a decrease in the disorderedness of the BITSH-1- thiophene interphase. The decrease in adsorption efficiency with an increase in the temperature denotes that the system is stable at standard temperature for high adsorption efficiency. The chemical potential of the thiophene is given as,

$$\mu = \mu^0 + RT \ln a \tag{10}$$

In dilute lower concentrations of adsorbate solution at mg L^{-1} levels, activity (a) is directly proportional to the concentration of thiophene, which can be related to standard Gibbs's free energy and reaction Gibb's free energy as,

$$\Delta G_r = \Delta G_r^0 + RT \ln \frac{[\text{thiophene}]_{\text{BITSH-1 MOF surface}}}{[\text{DBT}]_{\text{solution}}} \tag{11}$$

When $\Delta G_r = 0$ at equilibrium, this can be expressed as $\Delta G_r^0 = -RT \ln K_{eq}$, where

$$K_{eq} = \frac{[\text{thiophene}]_{\text{BITSH-1 MOF surface}}}{[\text{thiophene}]_{\text{solution phase}}} \tag{12}$$

The change in Gibb's free energy was found to be negative (-1.423 kJ mol^{-1}) confirming that the reaction is feasible or favourable and spontaneous with a negative change in enthalpy (-88 kJ mol^{-1}). The adsorption of thiophene on BITSH-1 is enthalpically more favourable.

Experimental variables, such as adsorbent (MOF) dosage, time and temperature that control the adsorption process as discussed are summarized and given in Fig. 5.

2.3. Comparative studies of BITSH-1 with other related materials for the desulfurization of thiophene

The proposed BITSH-1 material for thiophene adsorption was compared with previously reported MOFs and other related materials in terms of adsorption capacity, as listed in Table 1.[13,23–29] It is noteworthy that BITSH-1 shows a better adsorption capacity of 95.38 mg g^{-1} with comparatively lower time consumption at room temperature and without any oxidation of fuel compared to various other materials. Indeed, no further functionalization of MOF is required in the present system. Hence, the proposed MOF adsorbent with reactive metal sites and an appropriate pore size with high affinity towards sulfur removal shows good potential for the desulfurization of thiophenic model fuel.

2.4. Reusability of the BITSH-1 adsorbent

An important property of any adsorbent is the ease of reusability of the adsorbent material by desorbing adsorbed molecules by different physical or chemical factors. Solvent elution methods are generally performed for the desorption of sulfur-based compounds from MOF materials.[26] In the present case, thiophene was desorbed from BITSH-1 by heating the material at

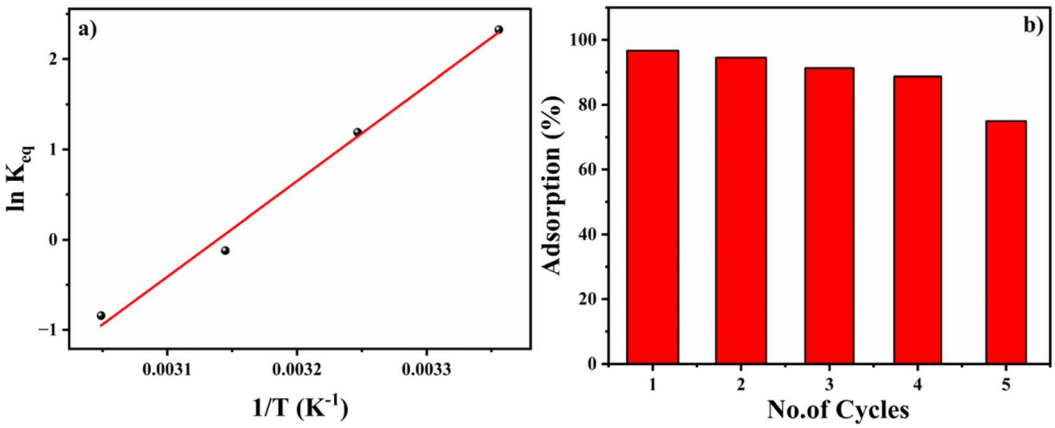

Fig. 6 (a) Van't Hoff plot for the adsorption of thiophene on BITSH-1. (b) Regeneration cycle of BITSH-1.

Table 1 Comparison of Langmuir adsorption capacities of reported MOF materials for adsorptive removal of sulfur with BITSH-1

Sl. No	MOF material	Adsorbate	Condition	Adsorption capacity (q_{max}) mg g^{-1}	Reference
1	MOF-199 (Cu-BTC)	Thiophene	4 h; 10 mL 0.2 g, 1000 mg L^{-1}	18 (thiophene)	16
2	MOF-199	DBT	30 s, 5 mL, 0.18 g, 50 mg L^{-1}	1.316 (S)	27
3	HKUST-1	BT	2 h, 20 mg 1500 mg L^{-1}, 500 μL	15.96 (S)	13
4	MIL-100	DBT	100 mg L^{-1}, 50 mg, 5 mL	6.50	28
5	MIL-101 Cr, PTA-MIL 101 Cr	DBT	500 mg L^{-1} S, 8 h	32, 136.5	15
6	HKUST-1	Thiophene	100 mg, 5 mL, 3 h, 100 mg L^{-1}	27	29
7	NENU-511	BT	5 mg, 2 mL, 1020 mg L^{-1} S, 12 h	54.53	30
8	Zn/Co bimetallic MOF derived porous carbon	DBT	40 mg, 20 mL, 4 h, 500 mg L^{-1}	40.6	31
9	4CuCl@MIL-101(Cr)	Thiophene	550 mg L^{-1}, 0.33 g	18.4	32
10	**BITSH-1**	**THIOPHENE**	**20 mg, 3 h, 50 mg L^{-1}, 10 mL**	**95.38 (thiophene)**	This study

100 °C (above the boiling point of thiophene, which is 84 °C) for 2 h. After heating, the structural integrity of the material was confirmed with the help of PXRD (Fig. S2†). The framework was found to be intact and suitable for carrying out the next cycle of adsorption. High adsorption efficiency was observed up to 4 cycles, which gradually decreased to 70% in the fifth cycle (shown in Fig. 6b). This could be ascribed to the active sites becoming saturated with weakening of BITSH-1 and thiophene interactions on repeated cycles.

2.5. Evidence of thiophene adsorbed on BITSH-1

The adsorption process depends mostly on the surface characteristics, such as the specific surface area, pore diameter and pore volume of the MOF material. Thiophene, which has a diameter of 4.5 Å, is easily adsorbed and accumulates in the pores of the framework. The driving force for the high adsorption capacity of thiophene on the MOF can be attributed to weak interactions between the MOF and thiophene molecules, which was confirmed with FTIR, XPS, TGA, XRF and single crystal data. N_2 sorption experiments were performed on BITSH-1 after the adsorptive desulfurization of thiophene. Fig. S3(c) and (d)† clearly show a decrease in the uptake of N_2. This is due to the insufficient number of pores after the accumulation of the adsorbed thiophene molecules in the MOF pores. This resulted in a decrease in pore volume and specific surface area of BITSH-1 after thiophene adsorption, as given in Table 2.

The PXRD confirmed that the crystallinity and integrity of the framework were retained even after the adsorption experiments (Fig. S2b†). The TGA graph of the thiophene-adsorbed MOF exhibits a weight loss around 83 °C attributed to the loss of thiophene molecules that have been adsorbed in the MOF pores (Fig. S4a†). This is supported by an endothermic peak at 80 °C in DTA pertaining to the release of the thiophene molecules that shows thiophene has been adsorbed by the MOF material (Fig. S4b†). XPS studies were performed to identify the elemental composition and their oxidation states. Fig. 7a shows the XPS survey spectra of BITSH-1 with characteristic binding energy peaks of Co, C, O and N elements. The XPS survey spectra of BITSH-1 after adsorption of thiophene confirms the presence of sulfur along with the other elements. Fig. 7b shows the deconvoluted spectra of sulfur S 2p with aromatic sulfur peaks at 162.89 and 165.62 eV, ascertaining the adsorption of thiophene on the MOF. The deconvoluted spectra of Co 2p in Fig. 7(c) and (d) confirm the +2-oxidation state of cobalt. The peaks at 782.63 eV and 797.29 eV in before-adsorption spectra correspond to Co $2p_{3/2}$ and Co $2p_{1/2}$.[33] The shift of these peaks to 782.25 and 797.84 eV indicates the interactions of thiophene with the metal sites of the adsorbent. The deconvoluted spectra

Table 2 Comparison of BET surface characteristics of BITSH-1 before and after adsorption of thiophene

	Surface area ($m^2\ g^{-1}$)	Pore volume ($cm^3\ g^{-1}$)	Pore diameter (nm)	Volume of N_2 gas uptake ($cm^3\ g^{-1}$)
Before adsorption	349.07	0.125	0.8	85.33
After adsorption	42.86	0.014	0.8	10.91

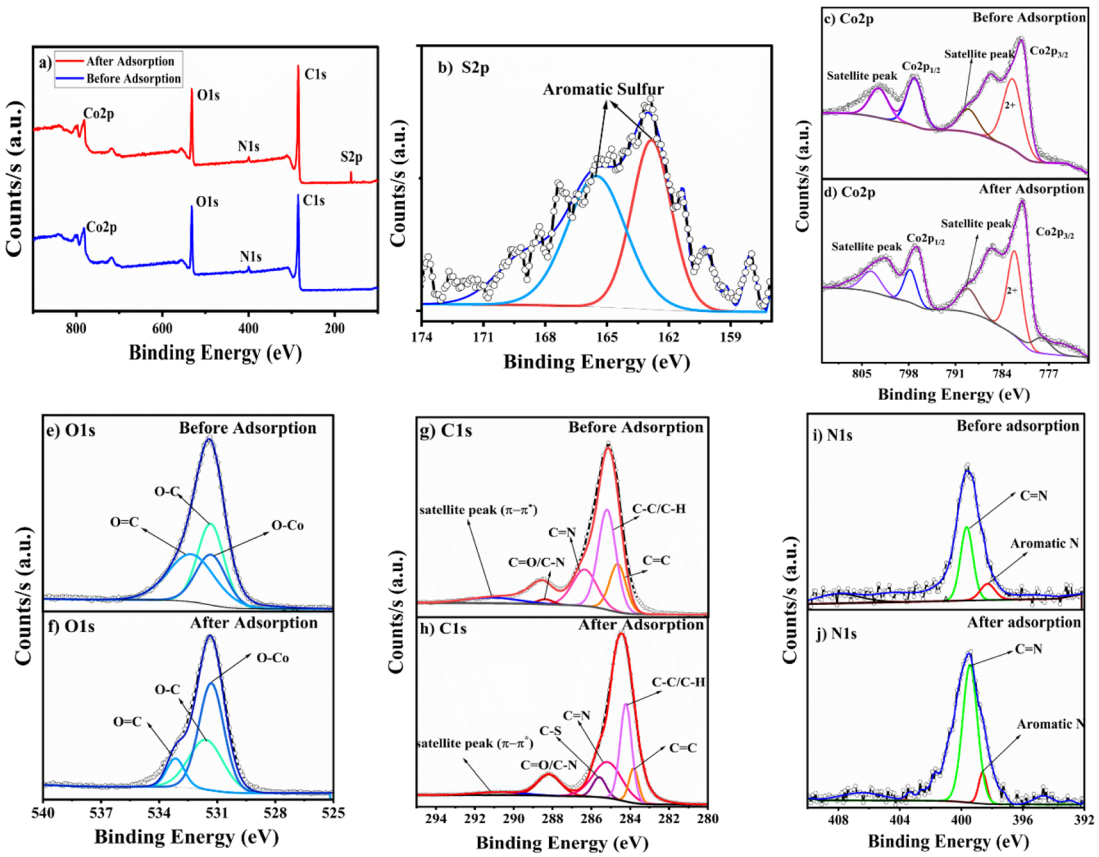

Fig. 7 (a) XPS survey scan spectra of BITSH-1 before and after adsorption. (b) S 2p deconvoluted spectra of BITSH-1 after adsorption. (c) and (d) Co 2p deconvoluted spectra of BITSH-1 before and after adsorption. (e) and (f) O 1s deconvoluted spectra of BITSH-1 before and after adsorption. (g) and (h) C 1s deconvoluted spectra of BITSH-1 before and after adsorption. (i) and (j) N 1s deconvoluted spectra of BITSH-1 before and after adsorption.

of C 1s of the adsorbent (Fig. 7g) give peaks at 284.57, 284.83, 285.84 and 288.94 eV that correspond to C=C, C–C/C–H, C=N, and C=O/C–N bonds. At 290.55 Ev, a satellite peak arises due to π–π^* electronic transitions in the organic framework of the MOF.[34] There is a noticeable increase in the intensity of this satellite peak in the spectra after adsorption, which confirms the π–π^* transition due to π–π interaction between adsorbed thiophene on the MOF. The shifts in these peaks (Fig. 7h) to 284.22, 284.71, 284.21, 285.21 and 288.28 eV correspond to a decrease in binding energy due to the adsorption of thiophene. When there are weak interactions of the lone pair of electrons on the sulfur atom in the thiophene molecule with C=O and C=C groups on the framework of BITSH-1 due to the electronegative nature of sulfur, the positive charge on carbon increases, which results in the reduction in the binding energy of C=O, C=C groups in the C 1s spectra of the framework.[35] A new peak at 285.60 eV after adsorption in the deconvoluted spectra corresponds to the C–S bond, confirming the presence of adsorbed sulfur. The N 1s deconvoluted spectra (Fig. 7(i) and (j)) show peaks at 398.25 and 399.69 eV corresponding to aromatic or pyridinic N and C=N in the MOF.[36] The O 1s deconvoluted spectra (Fig. 7(e) and (f)) show prominent peaks at 531.38, 531.41 and 532.48 eV corresponding to O–Co, O–C and O=C bonds in the framework.[37] There was no appreciable shift in O–Co (metal–oxygen) bonds after adsorption, pertaining to the fact that the metal linking with the framework remains stronger and intact even after adsorption, keeping the framework stable. XPS studies of BITSH-1 show satellite peaks of carbon corresponding to π–π interactions with an increase in the intensity after adsorption due to π interactions between the

aromatic rings of thiophene molecules and the MOF. The shift in binding energy in the Co $2p_{1/2}$ and Co $2p_{3/2}$ spectra specifies the electrostatic interaction of the Co^{2+} cation with the thiophene with a dipole moment of 0.55D.[38]

X-ray fluorescence analysis of the as-synthesized MOF material before and after adsorption of thiophene was performed for the qualitative measurement of Co and S elements. XRF analysis of the MOF material after adsorption of thiophene gave a distinct peak at an energy of 2.4 keV, confirming the presence of sulfur in the material along with Co Kα and Co Kβ at 6.9 and 7.6 keV, respectively (Fig. 8a).

The functional groups present in BITSH-1 were analysed from an FTIR study, as shown in Fig. 8b. A broad band at 3040 cm^{-1} corresponds to =C–H and C–H stretching vibrations. There is a shift in this stretching vibration to 3268 cm^{-1} on adsorption of thiophene. This is due to the presence of electronegative sulfur atoms that increase the C–H stretching frequency of MOF. The vibrational bands at 1594 and 1521 cm^{-1} correspond to asymmetric carboxyl group stretching. Prominent bands at 764 and 677 cm^{-1} can be attributed the Co–O stretching frequency observed after adsorption without any further shift.[39,40] A new band at 2880 cm^{-1} indicates the S–H bond in the thiophene moiety.[41] The presence of the S–H stretching band at 2880 cm^{-1} in BITSH-1 after adsorption of thiophene strongly confirms the presence of adsorbed thiophene along with stretching frequency bands corresponding to C=O, O–H and Co–O bands of the MOF network attributed to the interaction with thiophene. The increase in stretching frequency is due to the hydrogen-bonding interaction between the functional groups of BITSH-1 and the sulfur atom of thiophene.

2.6. Single crystal XRD

Single crystal X-ray studies were performed with thiophene-exchanged crystals to obtain direct evidence of host–guest interactions at the molecular level. A few good-quality crystals were selected and immersed in a vial containing 1 mL of thiophene and 5 mL of iso-octane, for 24 h. A suitable single crystal was then chosen to collect SCXRD data, which confirmed the presence of thiophene molecules inside the MOF pores. The thiophene-loaded BITSH-1 structure (BITSH-1-T) undergoes several dramatic changes compared with the as-synthesized BITSH-1 structure.[15] BITSH-1-T crystallizes in an orthorhombic crystal system with *Pbcn* space group (Table S4†). The asymmetric unit now contains one Co atom with full occupancy and another Co atom with 0.5 occupancy in addition to 1.5 units of BPDC and 0.5 unit of BPY linkers. One full thiophene molecule per asymmetric unit could be modelled inside the pores of the framework (Fig. 9(a) and (b), S5†). The thermal parameters of the thiophene molecule show large values owing to the movement of the molecule in channels. The thiophene molecule displays weak CH···HC van de Waals (vdW) interactions with the BPDC linker with a distance of 2.80 Å (Fig. 9b, Table S5†). Additionally, there are weak H-bonding interactions (2.91 Å, 2.94 Å, and 3.01 Å) present between the C–H group of the thiophene molecule and O atoms of the carboxylates of the BPDC linkers that explain the presence of thiophene closer to the cluster. Moreover, the S atom of the thiophene molecule is in proximity (3.25 Å) to the H atom of the BPY linker (Fig. 9b, Table S5†). In addition to one thiophene molecule that could be located with certainty, residual electron density was present in the channels that could not be modelled. This could be due to more thiophene molecule(s) but with a lower occupancy. The mask function of the Olex2 software[40] was used to remove the residual electron density (~30 electrons per asymmetric unit), which accounted for 0.7 thiophene molecules per asymmetric unit. Importantly, the SCXRD study confirms the presence of thiophene molecules inside the MOF channels, which explains the high selective uptake of thiophene by this MOF.

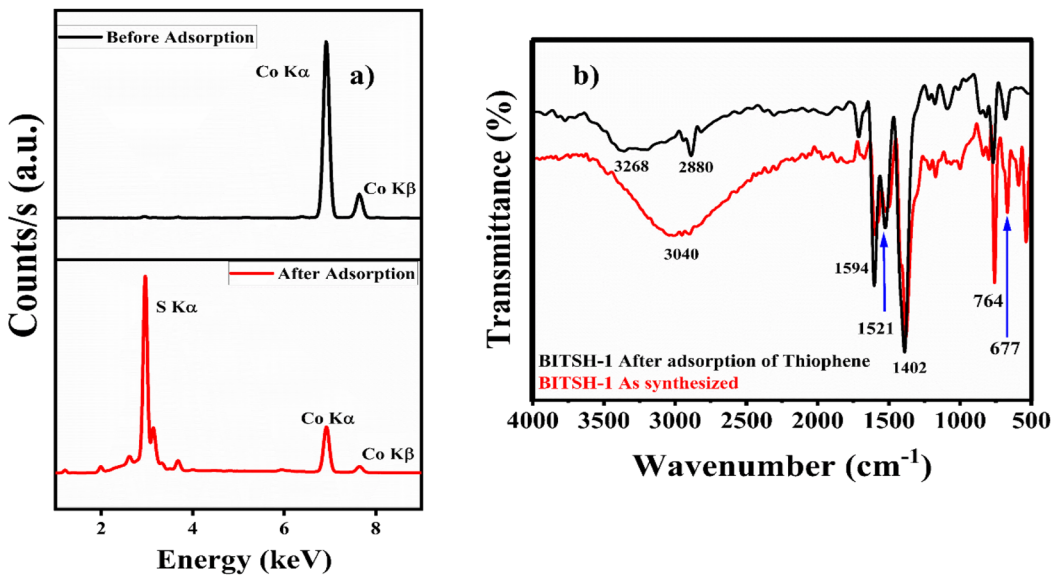

Fig. 8 (a) XRF spectra of BITSH-1 before and after adsorption. (b) FTIR spectra of BITSH-1 before and after adsorption.

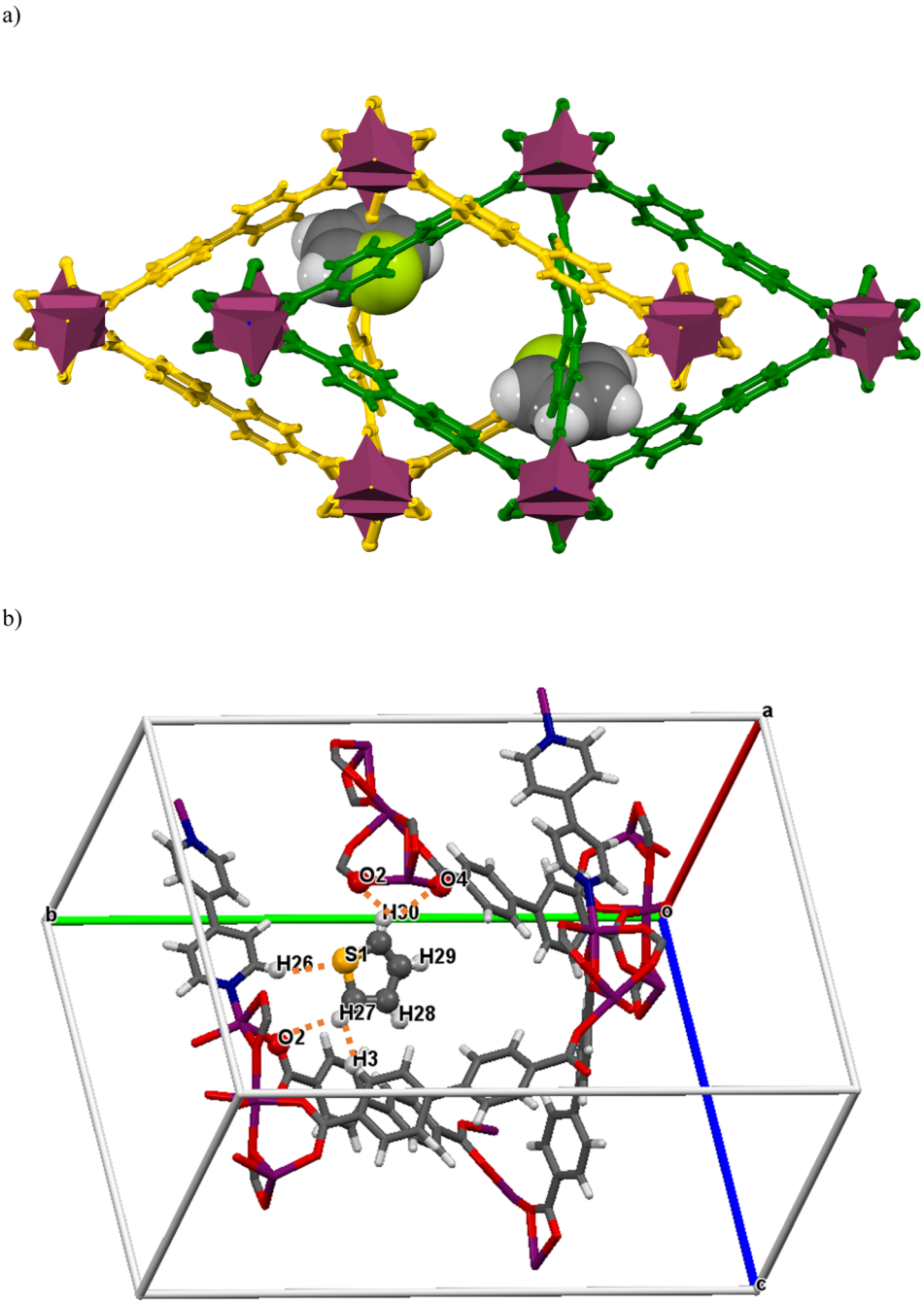

Fig. 9 (a) Packing diagram of BITSH-1 showing thiophene molecules encapsulated inside the pores of the 2-fold interpenetrated structure. C, H, and S atoms are represented in grey, white, and lime colours, respectively. (b) Packing diagram showing interactions between the BITSH-1 MOF structure and hiophene molecule.

2.7. Comparison of BITSH-1 adsorption for other SCCs (sulfur-containing compounds)

Comparative studies were carried out to check the selectivity and adsorption behaviour of BITSH-1 towards other sulfur compounds or higher thiophenic compounds, such as benzothiophene (BT) and dibenzothiophene (DBT) in the fuel. First, 50 mg L^{-1} of BT and DBT in a 10 mL volume iso-octane with 20 mg of adsorbent was incubated in an orbital shaker for 3 h. After adsorption, the concentration of BT and DBT in the solution was analysed through a UV absorption study, as shown Fig. 10(a) and (b). The percentage adsorption efficiency of BT on BITSH-1 was 40% and of DBT was 18%. The reduction in the adsorption efficiency can be attributed to kinetic diameters of benzothiophene (6 Å) and DBT (9 Å) with respect to the pore size of BITSH-1 (8 Å) restricting the accumulation of higher thiophene derivatives. Another reason could be the increase in electron cloud density on the S atom, which possibly restricts the interaction of the S atom

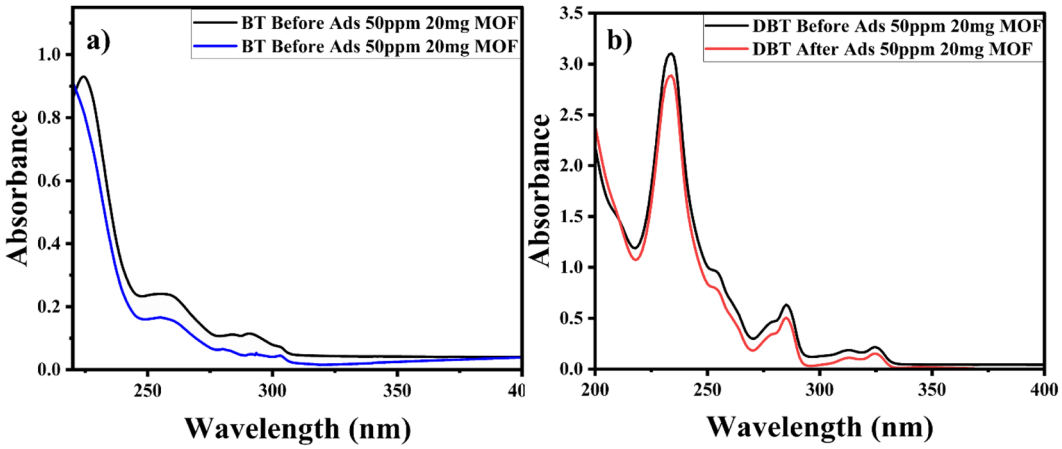

Fig. 10 UV-Vis spectra before and after adsorption of other sulfur-containing aromatic compounds with 20 mg adsorbent dosage and 50 mg L^{-1} concentration of (a) benzothiophene (BT) and (b) dibenzothiophene (DBT).

with the MOF material, resulting in lower efficiency of desulfurization.[42]

3. Conclusions

The synthesized BITSH-1 MOF was successfully applied for the adsorptive desulfurization of model fuel. The framework of BITSH-1 was found to exhibit excellent stability and strong interaction for the desulfurization of thiophene. The microporous nature of the framework with a specific surface area of 349.07 m^2 g^{-1} shows selective adsorption of thiophene with respect to other aromatic sulfur compounds. Single crystal XRD also revealed the selective uptake of thiophene. The experimental q_e (19.0 mg g^{-1}) was in good agreement with the theoretical value (19.99 mg g^{-1}) calculated from kinetics data. The adsorption was exothermic, with negative free energy and entropy change. The maximum adsorption capacity of BITSH-1 was found to be 95.38 mg g^{-1}, which was comparatively higher than in previous studies. This study highlights the evidence of adsorbed sulfur on the framework of BITSH-1 for up to four cycles.

Conflicts of interest

The authors declare that they have no known competing financial interests or personal relationships that could have appeared to influence the work reported in this paper.

Acknowledgements

The authors acknowledge the Central Analytical Laboratory, BITS Pilani, Hyderabad Campus, India for their support in analytical characterization techniques.

References

1 M. A. Betiha, A. M. Rabie, H. S. Ahmed, A. A. Abdelrahman and M. F. El-Shahat, *Egypt. J. Pet.*, 2018, **27**, 715–730.
2 J. Wang and J. Wei, *J. Mater. Chem. A*, 2017, **5**, 4651–4659.
3 D. Vashist, N. Kumar and M. Bindra, *Arch. Curr. Res. Int.*, 2017, **8**, 1–8.
4 W. Ahmad and I. Ahmad, *Mechanisms of Desulfurization by Nanomaterials*, 2018.
5 M. T. Timko, J. A. Wang, J. Burgess, P. Kracke, L. Gonzalez, C. Jaye and D. A. Fischer, *Fuel*, 2016, **163**, 223–231.
6 M. Rezakazemi and Z. Zhang, Desulfurization materials, *Comprehensive Energy Systems*, 2018, vol. 2, pp. 944–979.
7 G. Severa, J. Head, K. Bethune, S. Higgins and A. Fujise, *J. Environ. Chem. Eng.*, 2018, **6**, 718–727.
8 M. Ghassa, F. Khorashe, Z. Hajjar and S. Soltanali, *Energy Fuels*, 2023, **37**(9), 6490–6502.
9 Q. Huo, J. Li, G. Liu, X. Qi, X. Zhang, Y. Ning, B. Zhang, Y. Fu and S. Liu, *Chem. Eng. J.*, 2019, **362**, 287–297.
10 A. C. Elder, S. Bhattacharyya, S. Nair and T. M. Orlando, *J. Phys. Chem. C*, 2018, **122**, 10413–10422.
11 S. Sonal, P. Prakash, B. K. Mishra and G. C. Nayak, *RSC Adv.*, 2020, **10**, 13783–13798.
12 N. Ettekali, S. Allahyari, N. Rahemi and F. Abedini, *Microporous Mesoporous Mater.*, 2021, **326**, 111376.
13 K. A. Cychosz, A. G. Wong-foy and A. J. Matzger, *J. Am. Chem. Soc.*, 2008, **130**(22), 6938–6939.
14 G. Abdi, M. Ashokkumar and A. Alizadeh, *Fuel*, 2017, **210**, 639–645.
15 S. Jia, Y. Zhang, Y. Liu, F. Qin, H. Ren and S. Wu, *J. Hazard. Mater.*, 2013, **262**, 589–597.
16 A. A. Alyassiry and R. T. A. Alrubaye, *AIP Conf. Proc.*, 2020, **2213**, 020090.
17 T. Leelasree and H. Aggarwal, *J. Mater. Chem. C*, 2022, **10**, 2121–2127.
18 C. I. Sainz-Díaz, M. Francisco-Márquez and A. Vivier-Bunge, *Theor. Chem. Acc.*, 2009, **125**, 83–95.
19 M. Christina Nilavu, B. Arunraj, H. Aggarwal and N. Rajesh, *Fuel*, 2022, **324**, 124472.
20 B. Arunraj, V. Rajesh and N. Rajesh, *J. Rare Earths*, 2023, **41**, 157–166.

21 E. Ajenifuja, J. A. Ajao and E. O. B. Ajayi, *Appl. Water Sci.*, 2017, **7**, 3793–3801.
22 M. Christina Nilavu, B. Arunraj, H. Aggarwal and N. Rajesh, *Fuel*, 2023, **345**, 128172.
23 B. Arunraj, S. Talasila, V. Rajesh and N. Rajesh, *Sep. Sci. Technol.*, 2019, **54**, 1620–1631.
24 J. S. Piccin, G. L. Dotto and L. A. A. Pinto, *Braz. J. Chem. Eng.*, 2011, **28**, 295–304.
25 J. Kodali, S. Puram, P. Srinivas, M. C. Nilavu, B. Arunraj, A. S. Krishna Kumar and R. Nagarathnam, *Sep. Sci. Technol.*, 2023, 1–15.
26 M. Daneshvar and M. R. Hosseini, *Environ. Sci. Pollut. Res.*, 2018, **25**, 28654–28666.
27 C. Huang, R. Sun, H. Lu, Q. Yang, J. Hu, H. Wang and H. Liu, *Sep. Purif. Technol.*, 2017, **182**, 110–117.
28 L. Wu, J. Xiao, Y. Wu, S. Xian, G. Miao, H. Wang and Z. Li, *Sep. Purif. Technol.*, 2023, **306**(Part A), 122665.
29 F. Tian, Z. Fu, H. Zhang, J. Zhang, Y. Chen and C. Jia, *Fuel*, 2015, **158**, 200–206.
30 W. W. He, G. S. Yang, Y. J. Tang, S. L. Li, S. R. Zhang, Z. M. Su and Y. Q. Lan, *Chem.–Eur. J.*, 2015, **21**, 9784–9789.
31 Q. Huo, J. Li, G. Liu, X. Qi, X. Zhang, Y. Ning, B. Zhang, Y. Fu and S. Liu, *Chem. Eng. J.*, 2019, **362**, 287–297.
32 J. X. Shen, S. X. Mao, L. Wan, W. X. Wu, M. M. Jin, Y. X. Li, X. Q. Liu and L. B. Sun, *Sep. Purif. Technol.*, 2022, **290**, 120892.
33 C. Zhang, J. Xiao, L. Qian and S. Wang, *J. Mater. Chem. A*, 2016, **4**, 16516–16523.
34 D. N. G. Krishna and J. Philip, *Appl. Surf. Sci. Adv.*, 2022, **12**, 100332.
35 G. Zhou, E. Paek, G. S. Hwang and A. Manthiram, *Nat. Commun.*, 2015, **6**, 1–11.
36 D. Yu, O. Suarez, A. Itzel, O. Dy, O. S. Ai, B. Av and J. Gascon, *Langmuir*, 2017, **33**(50), 14278–14285.
37 G. Gao, X. Wang, Y. Ma, H. Rong, L. Lai and Q. Liu, *Ionics*, 2020, **26**, 5189–5197.
38 D. Peralta, G. Chaplais, A. Simon-Masseron, K. Barthelet and G. D. Pirngruber, *Energy Fuels*, 2012, **26**, 4953–4960.
39 T. Leelasree, S. Goel and H. Aggarwal, *ACS Appl. Nano Mater.*, 2022, **5**(11), 16753–16759.
40 A. Mishra, P. Chaturvedi, S. Datta, S. Sinukumar, P. Joshi and A. Garg, *Indian J. Med. Paediatr. Oncol.*, 2015, **36**, 24–31.
41 X. Zhu, M. Su, S. Tang, L. Wang, X. Liang, F. Meng and Y. Hong, *Mol. Vision*, 2012, 1973–1982.
42 A. Khodadadi Dizaji, H. R. Mortaheb and B. Mokhtarani, *Catal. Lett.*, 2019, **149**, 259–271.

